Time-Domain Finite Difference Approach to the Calculation of the Frequency-Dependent Characteristics of Microstrip Discontinuities

XIAOLEI ZHANG AND KENNETH K. MEI, FELLOW, IEEE

Abstract—**The frequency-dependent characteristics of the microstrip discontinuities have previously been analyzed using several full-wave approaches. The time-domain finite different (TD–FD) method presented in this paper is another independent approach and is relatively new in its application for obtaining the frequency-domain results for microwave components [26]. The purpose of this paper is to establish the validity of the TD–FD method in modeling circuit components for MMIC CAD applications.**

I. Introduction

MICROSTRIP discontinuities (Fig. 1) are the basic constituent elements of microstrip integrated circuits. The accurate modeling of these discontinuities using different numerical approaches is one of the most important topics in microwave CAD. The current cut-and-try cycles in the design of microstrip integrated circuits will be greatly reduced if the frequency-dependent characteristics of the discontinuities can be obtained with certainty. Using network concepts, various microstrip resonators, couplers, and filters can be directly analyzed from the interconnection of microstrip discontinuities and microstrip line segments.

The study of microstrip discontinuities started in the early 1960's. For nearly a decade, the analyses were mostly quasi-static in nature [1]–[12]. The first accurate full-wave frequency-dependent analysis appeared around 1975 [13]–[15]. This approach began with the use of a waveguide model with electric-wall top and bottom planes and magnetic-wall sides planes to characterize the microstrip. The effective dielectric constant of the filling and the width of the guide are assumed to be frequency dependent and are determined in such a way that the model and the actual microstrip line have the same frequency-dependent propagation constant and characteristic impedance. Using the waveguide model to represent the original microstrip, the fields at the region of the discontinuities are expanded into waveguide modes, and the modes of different regions are matched at intersection planes. From the matching coefficients the S matrix for different propagation modes can thus be calculated. The waveguide model approach is efficient and has reasonable accuracy for calculating the magnitude of the S parameters in the lower frequency range, but it is not able to take into account the radiation effect (since the model is a closed one) and the surface wave generation. Besides, the mode-matching step will also introduce error due to the fact that the actual modes excited in the microstrip discontinuities are not the same as those used in the model and accordingly will not match in exactly the same way. There is also an obvious limitation on the kinds of structures this method can be applied to. It cannot, for example, be used to analyze the microstrip open-end structure where one side of the discontinuity is not connected to a microstrip and where the radiation and surface waves are present.

A full-wave approach to the microstrip open end problem was first proposed by James and Henderson in 1979 [16]. The analysis on the far end of the microstrip open end, where the surface wave and the radiation wave are the constitutents of the fields, is carried out using an analytic mode-expansion technique. On the microstrip side, a TEM wave is taken as the dominant mode incident field, and the semiempirical results for the propagation constant and the characteristic impedance are used for this incident wave. The fields at both sides are matched at the interface and a variational step is taken to reduce the error introduced by the assumption of the TEM field pattern where the electric field has a vertical constant value under the strip and is zero elsewhere in the transverse plane. Mainly due to the roughness of the field pattern assumed, the results of this method are not very accurate, but the analysis did provide valuable physical insight.

Another important method which has been used by several investigators to model the microstrip discontinuities is the spectral-domain approach [17]–[19]. In using this method to analyze the shielded or covered structures, the fields and currents involved are Fourier transformed (with respect to the space variables) into the so-called spectral domain. The shape of the current on the microstrip is assumed to be close to the actual current distribution and is easily Fourier-transformable. The spectral-domain components of the fields and currents are

Manuscript received May 3, 1988; revised July 29, 1988. This work was supported by the Office of Naval Research Under Contract N00014-86-K-0420.

The authors are with the Department of Electrical Engineering and Computer Sciences, University of California at Berkeley, Berkeley, CA 94720.

IEEE Log Number 8823766.

0018-9480/88/1200-1775$01.00 ©1988 IEEE

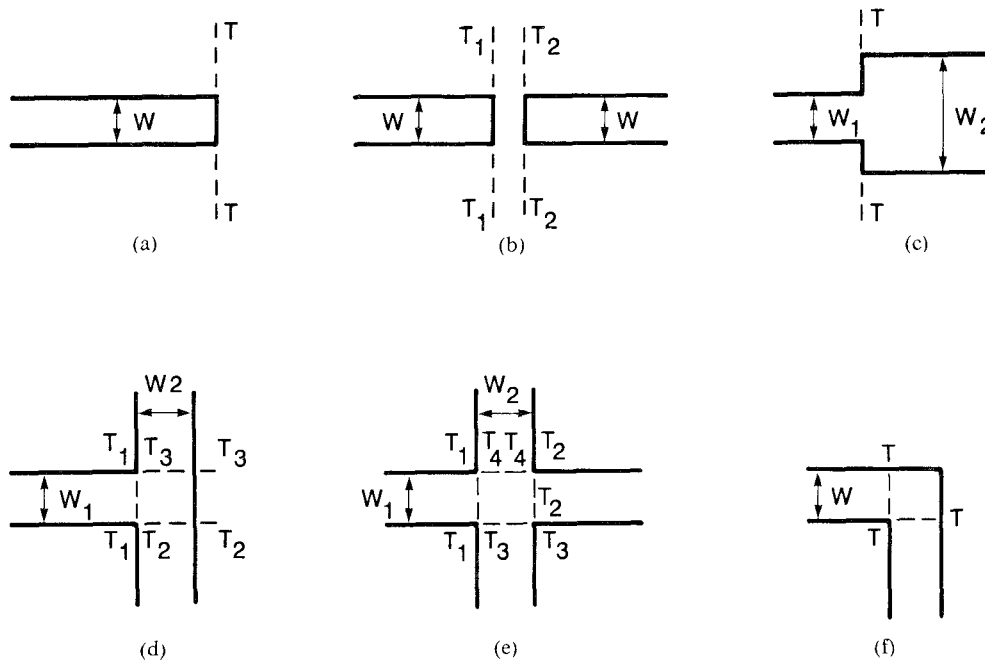

Fig. 1. Microstrip discontinuities. (a) Open-end. (b) Gap. (c) Step-in-width. (d) T junction. (e) Cross-junction. (f) Bend.

related according to the field continuity and boundary conditions and thus set up a system of equations for the variables. The inverse-transformed field solutions are used to calculate the S parameters.

Although a relatively accurate method for the type of components it is capable of calculating, the spectral-domain approach depends strongly on the current distributions assumed, which in many cases are hard to specify with high accuracy; thus it is limited in its applications. Besides, the frequency range which can be dealt with by this method is limited due to the difficulties which arise near the cutoff frequency of the higher order mode of the microstrip.

In recent years, the moment method has also been used by several investigators [20], [21] on the discontinuity problems. This method could in principle be an accurate one with wide applications, but due to the complexity of the Green's functions for the microstrip configurations it is not economical to make very fine numerical divisions to the microstrip for accurate results. In fact in many cases only a rational function form is used to represent the transverse current distribution on the microstrip, which may not correspond to the actual current distribution up to a certain frequency.

All the above-mentioned investigations are done in frequency domain; that is, the data for the whole frequency range are calculated one frequency at a time. It is an expensive task when the results of a wide frequency range are sought. This led us to seek an alternative way of calculating the frequency-domain data. Since a pulse response contains all the information of a system for the whole frequency range, it is a natural approach to use a pulse in the time domain to excite the microstrip structures, and from the time-domain pulse response to extract the frequency-domain characteristics of the system via the Fourier transform [26].

One numerical scheme which can be used to calculate the time-domain fields is the time-domain finite difference (TD–FD) method. It was first proposed by K. S. Yee in 1966 [22] and has been used by many investigators to solve electromagnetic scattering problems. Other numerical methods which can be used to solve this type of initial boundary value problem include the TLM method and Bergeron's method. Among these methods the TD–FD method is the most direct from a mathematical point of view, and is especially suitable for the accurate calculation of the microstrip fields, the reasons for which will be explained below.

Early investigators used the time-domain methods as a tool to obtain qualitative results that graphically illustrate the field propagation rather than to obtain design data via the Fourier transform of time domain results [24], [25]. In the process of our investigation, it has been found [26] that the Fourier transform of the time-domain results is very sensitive to numerical errors, notably those resulting from the imperfect treatment of the absorbing boundary conditions used to truncate the numerical computations of an open structure. Thus, even though the time-domain results may be reasonably accurate, the frequency-domain results obtained from their Fourier transform may not be acceptable as useful data.

The present available absorbing boundary conditions for the discretized wave equations are either not good enough in quality or require impractically large computer memories. Recently, a new type of absorbing boundary algorithm has been developed [29], [30] which can greatly improve the quality of the local absorbing boundary conditions. Using this new boundary treatment, together with a

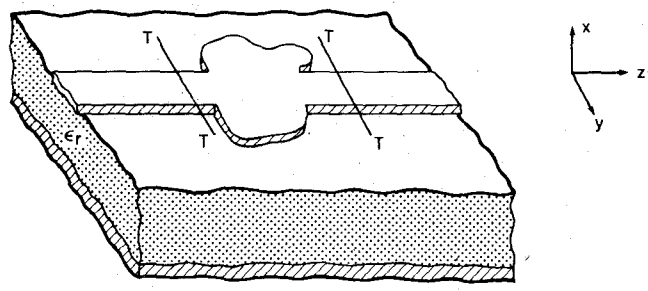

Fig. 2. A generalized microstrip discontinuity.

large enough computation domain, an accurate time-domain field can be obtained which can be used in the following Fourier transform step.

The calculated frequency-domain design data were compared with the available published results. These comparisons further demonstrate that the TD–FD approach is a viable method for modeling microstrip components.

II. Formulation of the Problem and the Numerical Method

A. General Formulation of the Problem

The generalized microstrip discontinuity under investigation is shown in Fig. 2 (a more general one will be an N-port structure instead of a two-port), where the strip and the bottom plane are made of a perfect conductor ($\sigma = \infty$) and the substrate has a relative dielectric constant of ϵ_r. The structure is assumed to be in an open environment, that is, above the dielectric and the metal strip surface, free space is assumed to extend to infinity; in the horizontal direction, apart from the discontinuity region, the substrate-ground structure also extends uniformly into infinity.

The Maxwell equations governing the solution of this problem are

$$\frac{\partial \vec{E}}{\partial t} = \frac{1}{\epsilon_i} \nabla \times \vec{H}$$

$$\frac{\partial \vec{H}}{\partial t} = -\frac{1}{\mu_0} \nabla \times \vec{E} \qquad (1)$$

where $i = 1, 2$ represents the substrate and the free-space region, respectively. At the interface of the two regions, the field continuity conditions are enforced.

For the uniqueness of the solution of these Maxwell equations, the following conditions must be satisfied:

a) The initial condition for the fields must be specified on the whole domain of interest; that is, $\vec{E}(\vec{r}, t = 0)$ and $\vec{H}(\vec{r}, t = 0)$ must be given everywhere inside the computation domain.

b) The tangential components of $\vec{E}$ and $\vec{H}$ on the boundary of the domain of interest must be given for all $t > 0$. For the boundary at infinity, Sommerfeld's radiation condition must be satisfied; that is, the wave at infinity must be of an outgoing type.

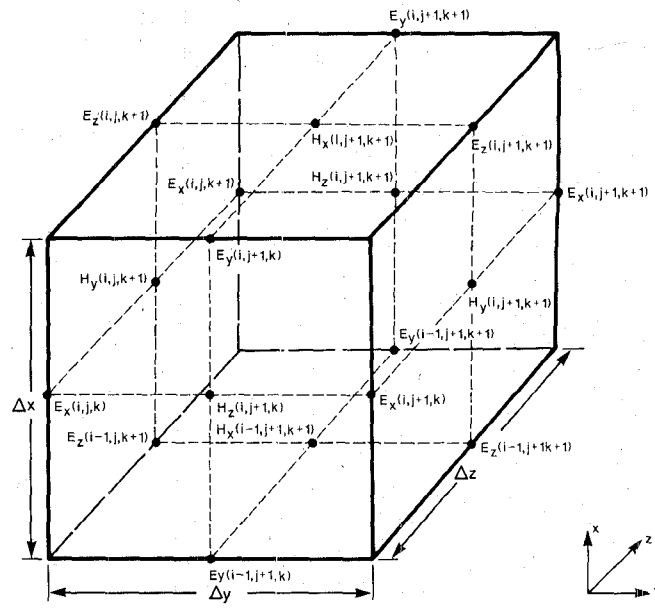

Fig. 3. Yee's mesh.

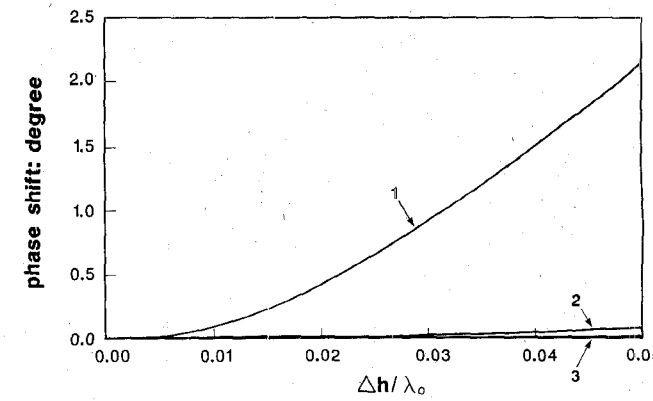

Fig. 4. Comparison of the numerical and microstrip dispersions (phase shift per time step): 1: microstrip dispersion ($w/h = 1.5$, $\epsilon_r = 13$); 2: leapfrog scheme, $c\Delta t/\Delta h = 1/7$; 3: a fourth-order scheme, $c\Delta t/\Delta h = 1/7$ [27].

B. The Time-Domain Finite Difference Algorithm

There are many ways to solve the system of Maxwell equations in (1) numerically. The TD–FD algorithm is one of the most suitable schemes for the purpose of this investigation.

To simulate the wave propagation in three dimensions, Yee [22] arranged the spatial nodal points, where different components of $\vec{E}$ and $\vec{H}$ are to be calculated, as in Fig. 3. The repetitive arrangement of the cells of Fig. 3 fills the computation domain with a finite difference mesh. Every component of $\vec{H}$ can be obtained by the loop integral of $\vec{E}$ using the four surrounding $\vec{E}$ nodal values according to Maxwell's curl equation for $\vec{E}$. A similar approach holds for the calculation of $\vec{H}$.

In this algorithm, not only the placement of the $\vec{E}$ and $\vec{H}$ nodes are off in space by half a space step, but the time instants when the $\vec{E}$ or $\vec{H}$ fields are calculated are also off by half a time step. To be more specific, if the components of $\vec{E}$ are calculated at $n\Delta t$, where Δt is the discretization unit in time, or the time step, and n is any nonnegative

integer, the components of $\vec{H}$ are calculated at $(n+1/2)\Delta t$. For this reason, this algorithm is also called the leapfrog method.

To summarize, for a homogeneous region of space, the discretization of the Maxwell curl equations (1) leads to the following:

$$E_x^{n+1}(i,j,k) = E_x^n(i,j,k) + \frac{\Delta t}{\epsilon} \cdot \left[\frac{H_z^{n+1/2}(i,j+1,k) - H_z^{n+1/2}(i,j,k)}{\Delta y} - \frac{H_y^{n+1/2}(i,j,k+1) - H_y^{n+1/2}(i,j,k)}{\Delta z} \right]$$

$$E_y^{n+1}(i,j,k) = E_y^n(i,j,k) + \frac{\Delta t}{\epsilon} \cdot \left[\frac{H_x^{n+1/2}(i,j,k+1) - H_x^{n+1/2}(i,j,k)}{\Delta z} - \frac{H_z^{n+1/2}(i+1,j,k) - H_z^{n+1/2}(i,j,k)}{\Delta x} \right]$$

$$\cdot E_z^{n+1}(i,j,k)$$

$$= E_z^n(i,j,k) + \frac{\Delta t}{\epsilon} \cdot \left[\frac{H_y^{n+1/2}(i+1,j,k) - H_y^{n+1/2}(i,j,k)}{\Delta x} - \frac{H_x^{n+1/2}(i,j+1,k) - H_x^{n+1/2}(i,j,k)}{\Delta y} \right]$$

$$H_x^{n+1/2}(i,j,k) = H_x^{n-1/2}(i,j,k) - \frac{\Delta t}{\mu} \cdot \left[\frac{E_z^n(i,j,k) - E_z^n(i,j-1,k)}{\Delta y} - \frac{E_y^n(i,j,k) - E_y^n(i,j,k-1)}{\Delta z} \right]$$

$$H_y^{n+1/2}(i,j,k) = H_y^{n-1/2}(i,j,k) - \frac{\Delta t}{\mu} \cdot \left[\frac{E_x^n(i,j,k) - E_x^n(i,j,k-1)}{\Delta z} - \frac{E_z^n(i,j,k) - E_z^n(i-1,j,k)}{\Delta x} \right]$$

$$H_z^{n+1/2}(i,j,k) = H_z^{n-1/2}(i,j,k) - \frac{\Delta t}{\mu} \cdot \left[\frac{E_y^n(i,j,k) - E_y^n(i-1,j,k)}{\Delta x} - \frac{E_x^n(i,j,k) - E_x^n(i,j-1,k)}{\Delta y} \right] \quad (2)$$

where Δx, Δy, and Δz are the space discretization units in the x, y, and z directions, respectively, and Δt is the time discretization interval. The numbering of the different $\vec{E}$ and $\vec{H}$ components is illustrated in Fig. 3, which is different from that in Yee's original paper due to programming considerations.

The TD–FD algorithm has several advantages over other schemes for the calculation of microstrip time-domain fields. First, the central difference nature of the leapfrog method makes it a relatively accurate method (second-order accuracy in both time and space), compared to other first-order schemes. Second, there is no need for special treatment of the edge of the microstrip if the tangential $\vec{E}$ and vertical $\vec{H}$ components are arranged on the metal strip and only the parallel components of the electric field are arranged on the edge of the strip. Finally, the leapfrog algorithm has the unique characteristics that the numerical scheme has no dissipation (amplitude increase or decrease for any frequency component) and only a small amount of dispersion [27]. It has been shown [28], [29] that the numerical dispersion is negligible compared to the physical dispersion of the microstrip structure, as seen in Fig. 4 for comparing the microstrip dispersion and numerical dispersions for the leapfrog scheme and for a fourth-order finite difference scheme used to solve the one-dimensional wave equation. (The actual frequency range of interest for the microstrip discontinuity problems corresponds to $\Delta h/\lambda_0 \approx 0$–$0.03$.) Thus, no higher order finite difference is needed for the accurate modeling of the microstrip structures.

For any finite difference scheme, a stability condition must be found which guarantees that the numerical error generated in one step of the calculation does not accumulate and grow. The stability criterion of Yee's algorithm is the Courant condition [23]:

$$v_{\max} \cdot \Delta t \leq \frac{1}{\sqrt{\frac{1}{\Delta x^2} + \frac{1}{\Delta y^2} + \frac{1}{\Delta z^2}}}. \quad (3)$$

For the special case of $\Delta x = \Delta y = \Delta z = \Delta h$, (3) becomes

$$v_{\max} \cdot \Delta t \leq \frac{1}{\sqrt{3}} \cdot \Delta h. \quad (3a)$$

where $v_{\max}$ is the maximum signal phase velocity in the configuration being considered.

The stability of the absorbing boundary condition cannot be achieved exactly due to the imperfection of nearly all the presently available absorbing boundary conditions for the numerical solution of wave equations (there will always be some unrealistic reflection wave going back to the computation domain due to the boundary treatment). But since the computation lasts for only a limited time, one can always minimize the influence of the unrealistic reflections by making the computation domain sufficiently large and stopping the computation after the useful information has been obtained.

C. Choice of the Excitation Pulse

The excitation pulse used in this investigation has been chosen to be Gaussian in shape. A Gaussian pulse has a smooth waveform in time, and its Fourier transform (spectrum) is also a Gaussian pulse centered at zero frequency. These unique properties make it a perfect choice for investigating the frequency-dependent characteristics of the microstrip discontinuities via the Fourier transform of the pulse response.

An ideal Gaussian pulse which propagate in the $+z$ direction will have the following expression:

$$g(t,z) = \exp\left[-\frac{\left(t - t_0 - \dfrac{z - z_0}{v}\right)^2}{T^2}\right] \tag{4}$$

where v is the velocity of the pulse in the specific medium, and the pulse has its maximum at $z = z_0$ when $t = t_0$.

The Fourier transform of the above Gaussian pulse has the form

$$G(f) \propto \exp\left[-\pi^2 T^2 f^2\right]. \tag{5}$$

The choices of the parameters T, t_0, and z_0 are subject to two requirements. The first is that after the space discretization interval Δz has been chosen fine enough to represent the smallest dimension of the structure and the time discretization interval Δt has been chosen small enough to meet the stability criterion (3), the Gaussian pulse must be wide enough to contain enough space divisions for a good resolution. And at the same time, the spectrum of the pulse must be wide enough (or the pulse must still be narrow enough) to maintain a substantial value within the frequency range of interest. If these last two conditions cannot be satisfied simultaneously, Δz has to be rechosen to be even smaller.

The pulse width W chosen in this work is approximately 20 space steps. We define the pulse width to be the width between the two symmetric points which have 5 percent of the maximum value of the pulse. Therefore, T is determined from

$$\exp\left[-\frac{\left(\dfrac{W}{2}\right)^2}{(vT)^2}\right] = \exp(-3)(\approx 5\%) \tag{6}$$

or

$$T = \frac{1}{\sqrt{3}} \cdot \frac{10\Delta z}{v}. \tag{7}$$

By making this choice of T, the maximum frequency which can be calculated is

$$f_{\max} = \frac{1}{2T} \qquad \left(G\left(\frac{1}{2T}\right) \approx 0.1\right) \tag{8}$$

$$= \frac{1}{2} \cdot \frac{\sqrt{3}\,v}{10\Delta z} \tag{9}$$

which, with the specific Δz chosen, is high enough to cover the entire frequency range of interest, as will be shown below in the discussion of the numerical results.

The second requirement is that the choice of z_0 and t_0 be made such that initial "turn on" of the excitation will be small and smooth.

Another consideration in excitation is the specification of the spatial distribution of the field on the excitation plane. Ideally, the use of the dominant mode distribution is preferred. But this distribution is generally not known with high enough accuracy. By the use of our knowledge of the modes in the microstrip structure, a very simple field distribution can be specified at the excitation plane which serves our purposes almost as well.

The tangential electric field to be specified on the excitation plane is assumed to have only the E_x component, which is distributed uniformly under the strip and is zero elsewhere. This is not the exact dominant mode field distribution, although in the latter case the energy is also concentrated under the strip. But for frequencies under the cutoff frequency of the first waveguide type higher order mode and below the strong coupling frequency of the substrate modes (the lowest one of them will be referred to below as the inflection frequency), the only mode which can propagate down the microstrip is the dominant mode. The substrate modes which do not cut off at those frequencies have imaginary propagation (phase) constants with respect to the major wave propagation direction due to the presence of the metal strip and thus can only propagate sidewards. After the inflection frequency, there will be modes other than the dominant mode which can propagate down the line. But those modes will not contaminate our lower frequency results after the Fourier transform. This is due to the fact that the physical model and the numerical method we used are both linear; thus the modes at different frequencies will not couple energy from each other.

Therefore, as long as we allow a certain distance for the Gaussian pulse to propagate out of the excitation plane, and thus allow the unwanted substrate modes at lower frequencies to leave the central region of the microstrip, the low-frequency component of the pulse will consist of the dominant mode only. Graphically, the pulse pattern in the transverse direction gradually becomes stabilized (to its actual physical form) and a prominent edge effect manifests itself as the calculation goes on and the pulse is seen to propagate down the line.

Also, for the reasons mentioned above, caution must be taken when interpreting the Fourier transformed results after the inflection frequency, as the time-domain method does not have the capability of distinguishing between modes. These results do not correspond to the exact dominant mode results in general, although how great an influence the higher order modes have on the dominant mode results is still left to be determined.

D. Dielectric–Air Interface Treatment and the Artificial Absorbing Boundary Conditions

Fig. 5 shows the finite difference computation domain used for the discontinuity problems (in this case, a mi-

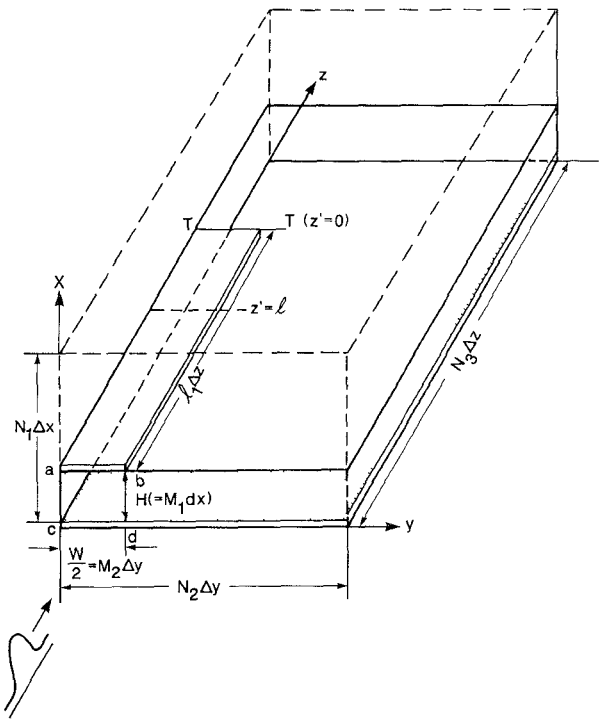

Fig. 5. Finite difference computation domain for microstrip open-end.

crostrip open end is shown as an example). Due to symmetry, only half of the structure is placed in the mesh domain with a magnetic wall at the plane of symmetry.

The finite difference form (2) of Maxwell's equations is derived in the uniform region of the medium and therefore cannot be applied to the nodal points on the dielectric–air interface or on the boundary planes of the finite difference mesh. All these points require special treatment.

The field components which lie on the dielectric–air interface are the tangential components of $\vec{E}$ (E_y and E_z) and the vertical component of $\vec{H}$ (H_x). In calculating H_x, (2) can still be used because the value of μ does not change across the boundary, and the E_y and E_z components used to calculate H_x are the tangential components with respect to the interface and are thus continuous across the boundary. To calculate E_y and E_z, however, a finite difference formulation other than (2) must be derived from the field continuity conditions across the boundary. The derivation is given in the Appendix, which is similar to that of Lin [31] for a two-dimensional finite element scheme, and the result is that E_y can be obtained by the discretization form of

$$\frac{\epsilon_1+\epsilon_2}{2}\cdot\frac{\partial E_y}{\partial t}=\frac{\partial H_x}{\partial z}-\frac{\Delta H_z}{\Delta x} \tag{10}$$

and E_z can be obtained through

$$\frac{\epsilon_1+\epsilon_2}{2}\cdot\frac{\partial E_z}{\partial t}=\frac{\Delta H_y}{\Delta x}-\frac{\partial H_x}{\partial y}. \tag{11}$$

In other words, the average value of ϵ is used in (2) for the calculation of the interface E_y and E_z nodes.

The values of E_y, E_z, and H_x vanish on the metal strip because of the assumption of a perfectly conducting surface. This also holds for the ground plane.

Since the computation domain cannot include the whole space, the finite difference mesh must be truncated to accommodate the finite computer memories. In solving our problems, the truncation planes are the side, top, and end surfaces (Fig. 5). The numerical algorithm on the truncation planes must simulate the propagation of the outgoing waves; this is known as the artificial absorbing (or radiation) boundary condition.

The perfect absorbing boundary conditions are usually global in nature, which makes them quite expensive to implement and requires excessively large computer memories. The local absorbing boundary conditions, which make use of only the fields at the neighboring space and time nodes, are relatively inexpensive to implement.

There are quite a few local absorbing boundary conditions available, but most of them are not "absorbing" enough for the purpose of this investigation. As mentioned in the Introduction, the Fourier transform of the time-domain results is very sensitive to the reflection errors. A small amount of reflection may not visibly influence the time-domain fields, but the transformed results could be far off.

To improve the local absorbing boundary conditions, a new approach based on the "local cancellation of the leading order errors" has been developed and shown to provide substantial improvement of absorbing qualities. The boundary treatment used in this investigation will be discussed below.

Consider the end boundary ($z = N_3\Delta z$) first. In most of the cases under consideration, the end surface will contain one end of the microstrip with its other end connected to the microstrip discontinuity. For most high-dielectric-constant substrates, owing to the guiding nature of the metal strip, the major direction of the power flow is in the $+z$ direction, or nearly normal incident. The sideways leakage and radiation are small. This is quite similar to a one-dimensional propagation case, and a natural choice of the boundary condition is to use the field values a few Δz before and a few Δt earlier for the present boundary fields.

In a microstrip structure, the existence of the dielectric substrate makes the wave velocity in the main propagation direction $+z$ be less than the velocity of light c in free space. Denote this velocity as v (usually v is some fraction of c and is also weakly dependent on frequency due to the dispersive nature of the structure). Assume $a_1 \cdot v = c$, where a_1 is a constant. (Rigorously speaking, it will be a weak function of frequency. Here for the purpose of the boundary treatment only its low-frequency value is adapted). For the stability criterion (3a) to be satisfied, we must have (choose $\Delta x = \Delta y = \Delta z = \Delta h$)

$$v_{\max}\Delta t = c\Delta t = a_1 v\Delta t \equiv k\Delta h \tag{12}$$

where k is a certain constant satisfing

$$k \leqslant \frac{1}{\sqrt{3}}$$

and therefore

$$v \cdot \Delta t = \frac{k}{a_1} \cdot \Delta h. \tag{13}$$

From (13) it is clear that we can always make the wave travel a certain integral number of space steps in some integral number of time steps by choosing a specific k (better to be less than but close to $1/\sqrt{3}$ for high accuracy), thus avoiding the need for interpolation, and the stability condition (3a) or (13) is still satisfied.

Take the 50 Ω line on the alumina substrate ($\epsilon_r = 9.6$, $W/H = 1.0$) as an example. Here $\epsilon_{reff}(f=0) \approx 6.6$; then $v = 1/\sqrt{6.6} \cdot c$, or $a_1 = \sqrt{6.6}$. If we choose $k = 0.514$, then k/a_1 will be approximately $1/5$; that is, the wave will travel one space step in approximately five time steps.

After choosing the parameters as above, the boundary value of the fields can now be specified as the value of the inner nodes at several time steps earlier. Again, for the alumina case, the boundary condition of the fields will be

$$E_t(N_3\Delta z, n\Delta t) = E_t[(N_3-1)\Delta z, (n-5)\Delta t] \tag{14}$$

where $E_t(N_3\Delta z, n\Delta t)$ is any electric field component which lies on the boundary of the computation domain (actually only the tangential components of the fields are needed for later calculations). By using this treatment, a storage of the next-to-boundary nodal fields for several time steps is needed. Since this is a storage of two-dimensional data, it will not increase the memory requirement significantly, compared to the major three-dimensional storage.

Usually, merely applying the boundary operation as above will still leave a visible (3–5 percent) amount of reflection. This is partly due to the fact that the true wave propagation is not one-dimensional, and partly because the velocity of the wave is not a constant but rather a function of frequency.

To improve the earlier boundary treatment, it is found that if we apply the same kind of boundary condition on the tangential $\vec{H}$ field next to the boundary, i.e. (for the alumina case),

$$H_t[(N_3-1/2)\Delta z, (n+1/2)\Delta t] = H_t[(N_3-3/2)\Delta z, (n+1/2-5)\Delta t] \tag{15}$$

and compare it with those $\vec{H}$ values calculated from the loop integration of $\vec{E}$ fields (here the boundary $\vec{E}$'s used are obtained in the previous computation step by using boundary condition (14)), these two $\vec{H}$ fields will always have the property that the errors contained in them due to the imperfect treatment of the boundary condition will have opposite signs and the magnitudes of these errors will maintain a known ratio. Therefore by a weighted average (1 : 5 in this case) of these two $\vec{H}$ fields, we can get an error cancellation effect and the resulting boundary operation will have a much improved quality. This kind of error cancellation approach can actually be applied to any kind of linear local boundary conditions. A general discussion of it for the one-dimensional case can be found in [30].

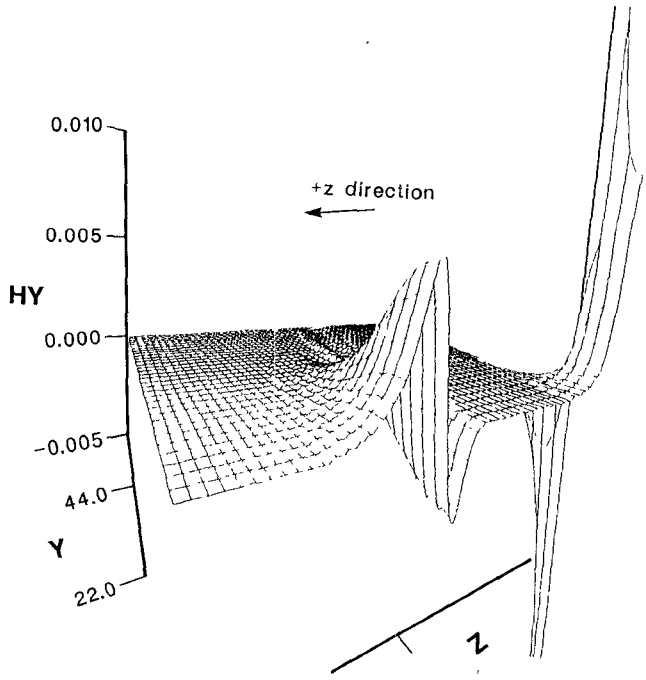

Fig. 6. dc magnetic field on the front surface due to the electric wall boundary treatment.

The treatment of the side boundary is similar to that of the end. But in this case the normal incident approximation is no longer valid. The direction of incidence of the wave changes with both time and position. An accurate and economic treatment of the side boundary condition has not been found so far. As a compromise, the boundary tangential $\vec{E}$ fields will always be given the value of their inner neighbors one time step earlier. A similar operation is done for the $\vec{H}$ nodes $1/2$ space step from the boundary, and the error cancellation algorithm still works in this case.

On the top plane, only the boundary condition for $\vec{E}$ fields is applied in the same way as for the side plane. The cancellation scheme does not work for the top plane, since the field is of the evanescent type in that direction.

The front surface needs some special treatment. During the time when the Gaussian pulse is excited, under the strip on plane *abcd* of Fig. 5, the vertical field is given the value of the Gaussian pulse. Elsewhere on the front surface the electric fields are fixed to be zero. This is equivalent to an electric wall boundary condition (the magnetic wall or symmetric boundary condition turned out not to be able to give a clear tail of the pulse). Following the passing of the pulse with part of it reflected back from the discontinuities, the front surface should now behave in a "transparent" way, as in the real case. This means that from the moment the reflected wave reaches the front surface a radiation type of boundary condition must be "switched on." It is found that the early enforced electric wall boundary condition induced a dc current or tangential magnetic field on the front surface and nearby (Fig. 6). This local dc field, although it has no influence on the traveling pulse, does cause trouble in the boundary treat-

ment. That is, if we switch on the radiation condition on this wall, the numerical errors will accumulate very rapidly and the solutions soon "blow up."

To solve this problem, what actually has been done is that after the pulse leaves the source plane and before it is reflected back from the discontinuities, the radiation boundary condition is switched on at a surface which is parallel to the source plane but a few space steps into the computation domain, and this is sufficient to avoid the trouble caused by the dc current.

At this stage, after all the boundary conditions have been properly treated, the numerical solution of the discontinuity problems is quite direct.

III. Numerical Results

In this investigation, five kinds of symmetric microstrip discontinuities on alumina substrate ($\epsilon_r = 9.6$) for a 50 Ω transmission system ($W/H = 1.0$, $W = 0.6$ mm) have been studied. They are (refer to Fig. 1) microstrip open-end, cross and T junctions, step-in-width and gap. Among these discontinuities, the microstrip open-end case has been given the most detailed discussion and compared with all the available published results.

A. Microstrip Open-End Terminations

A microstrip open-end on alumina substrate ($\epsilon_r = 9.6$) as shown in Fig. 5 is studied first. The parameters of the structure are as follows:

thickness of substrate: $H = 0.6$ mm
width of metal strip: $W = 0.6$ mm
thickness of metal strip: $t = 0.0$.

To accommodate the structural details of the microstrip, the mesh parameters have been chosen to be

space interval: $\Delta h = H/10 = 0.06$ mm;
$\Delta x = \Delta y = \Delta z = \Delta h$;
$N_1 = 40$, $N_2 = 120$, $N_3 = 190$;
$l_1 = 120$, $M_1 = 10$, $M_2 = 5$;
$l = 20, 30, 40, 50$ (Δh) have all been used to calculate the results for comparison;
time step $\Delta t = k \cdot \Delta h / c$ s, where c is the velocity of light in air and k is a constant restricted by the stability criterion (3);
$k = 0.514$ in this calculation.

A Gaussian pulse excitation is used at the front surface. It is uniform under the strip (in plane *abcd* of Fig. 4) and has only the E_x component with the following specified value:

$$E_x(t) = \exp\left[-\frac{(t-t_0)^2}{T^2}\right] \tag{16}$$

where $t_0 = 350\,dt$ and $T = 40\,dt$; elsewhere on the front surface, set $E_x = E_y = 0$. The pulse width in space is about $20dh$, which is wide enough to obtain good resolution. The frequency spectrum of this pulse is from dc to about 100 GHz.

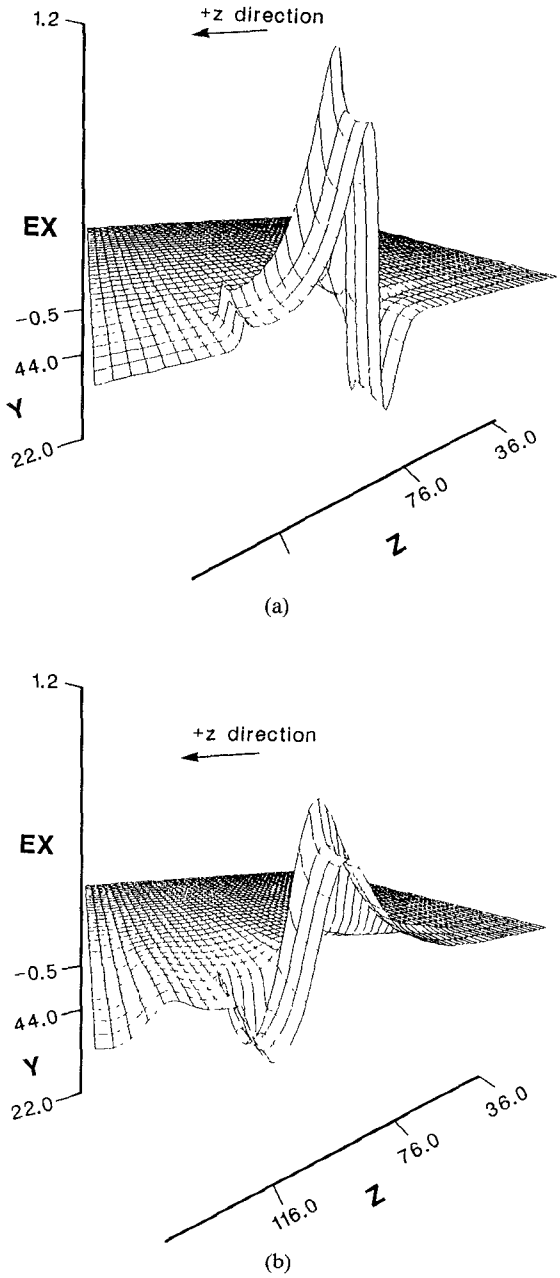

Fig. 7. Gaussian pulse propagation and reflection in the microstrip open-end structure: E_x component just underneath the strip. (a) Incident pulse just reaching the open end. (b) Pulse being reflected back and the surface wave being generated.

Fig. 7 shows the calculated time-domain field (E_x component) for a microstrip open end. The plane where the plot is drawn is just underneath the metal strip. Part (a) is the field distribution at the moment when the Gaussian pulse just reaches the open end and is reflected. The reflected wave is seen to have the same sign as the incident wave and is added to the incident wave. Part (b) shows the reflected wave and a small amount of traveling surface wave.

The microstrip open end structure is a one-port network (Fig. 5). Its scattering matrix has only one element, that is,

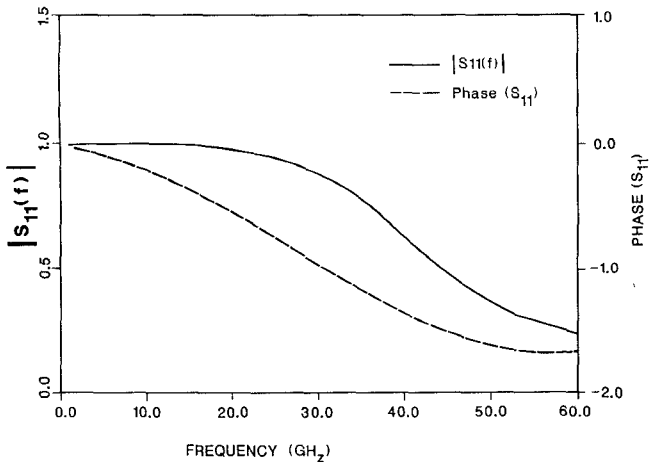

Fig. 8. Frequency-dependent S parameter of open end: magnitude and phase.

S_{11} or the reflection coefficient. S_{11} is defined as

$$S_{11}(f) = \frac{V_{\text{ref}}(f)}{V_{\text{inc}}(f)} \tag{17}$$

where $V_{\text{ref}}(f)$ is the transformed reflection voltage at the input plane (i.e., the reference plane $T-T$ in Fig. 5) of the one-port, and V_{inc} is the transformed incident voltage at the same position. In this calculation, the incident field is obtained from that of an infinitely long microstrip, and the reflected field from the open end is obtained from the difference between the total open-end field and the incident field.

It is common practice in microwave network calculation for S_{11} to be calculated away from the discontinuity through the transmission line formula (refer to Fig. 5.)

$$S_{11}(f) = \frac{V_{\text{ref}}(f, z'=l)\cdot e^{\gamma(f)l}}{V_{\text{inc}}(f, z'=l)\cdot e^{-\gamma(f)l}} = \frac{V_{\text{ref}}(f, z'=l)}{V_{\text{inc}}(f, z'=l)}\cdot e^{2\gamma(f)l}. \tag{18}$$

This is done here to allow the higher order, evanescent modes which were generated near the discontinuity to die out. They are not included in the calculation.

Fig. 8 shows the calculated results of the magnitude and phase of $S_{11}(f)$ for the open end under consideration. The uniqueness of the solution to the use of either the field at one point under the metal strip or the voltage between the strip and the ground, when substituted into (18) for the V's there, has been checked and found to be well satisfied. This is expected to be true once the mode distribution is well established on the line.

The equivalent circuit as shown in Fig. 9 with frequency-dependent circuit parameters is used to model the microstrip open end. Here

$$Y(f) = G(f) + j2\pi f C(f) \tag{19}$$

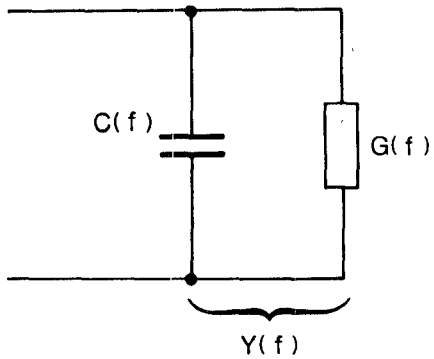

Fig. 9. Equivalent circuit of the microstrip open end.

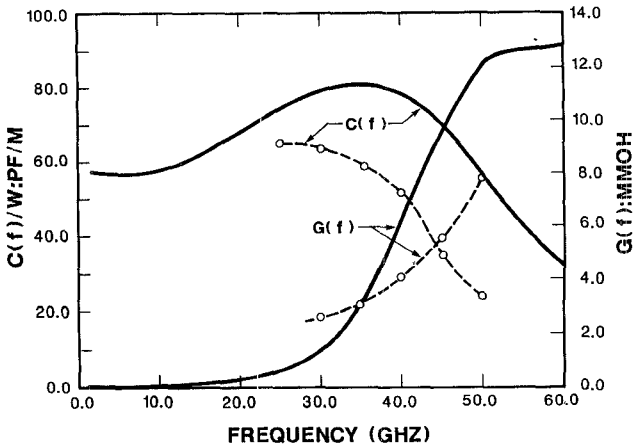

Fig. 10. Frequency-dependent equivalent circuit parameter $C(f)/W$ and $G(f)$ for open end. Solid lines denote time-domain results; dashed lines denote the results of Katehi and Alexopoulos [21].

and $Y(f)$ is related to $S_{11}(f)$ through

$$Y(f) = \frac{1 - S_{11}(f)}{1 + S_{11}(f)} \cdot \frac{1}{Z_0(f)}. \tag{20}$$

Here $Z_0(f)$ is the characteristic impedance of the microstrip, which is calculated using the ratio of voltage and current [26].

The calculated $C(f)$ and $G(f)$ are plotted in Fig. 10 together with the results presented by Katehi and Alexopoulos [21] for the same structure. The comparison shows quite an amount of discrepancy, especially for higher frequencies. Although both models should be questioned, there is an obvious question in the result of [21] for $G(f)$ in that it does not exhibit a trend to go smoothly down to zero as the frequency goes to dc. For $C(f)$, an equivalent parameter $\Delta l(f)$ can be derived from it and has been compared with extensive published results below.

The parameter which can also be used to account for the capacitive characteristic of the open end is the effective increase in length Δl. It is related to C through [32]

$$\frac{C(f)}{W} = \frac{\Delta l(f)}{h}\sqrt{\epsilon_{\text{eff}}}\,\frac{1}{Z_0(f)}\,\frac{h}{W} \tag{21}$$

where ϵ_{eff} is the effective dielectric constant of the microstrip [32].

The calculated $\Delta l(f)$, together with the comparison with several other published results, is given in Fig. 11.

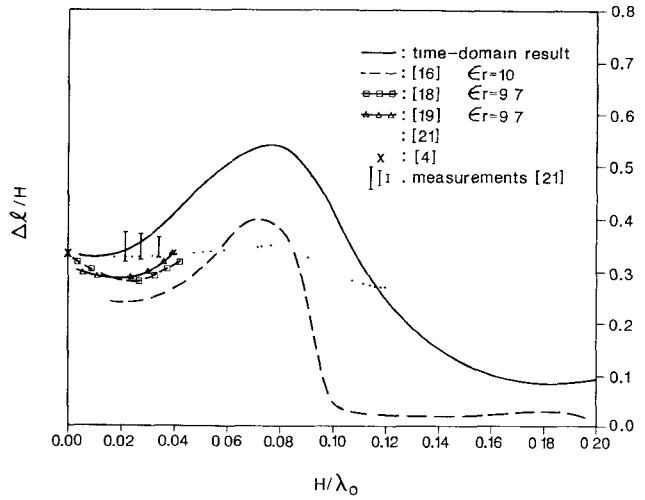

Fig 11. Effective length increase $\Delta l(f)/H$.

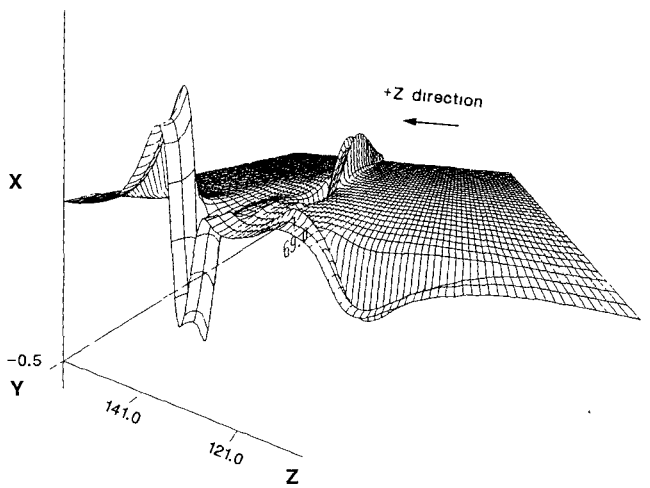

Fig. 12. Gaussian pulse propagation and reflection in the microstrip cross-junction: E_x component just underneath the strip.

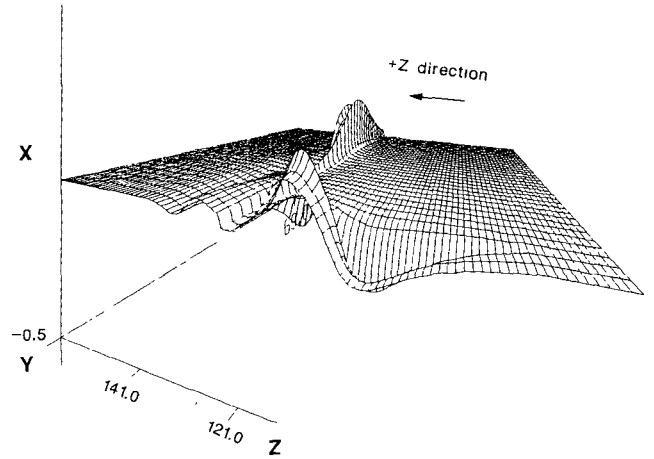

Fig. 13 Gaussian pulse propagation and reflection in the microstrip T junction: E_x component just underneath the strip.

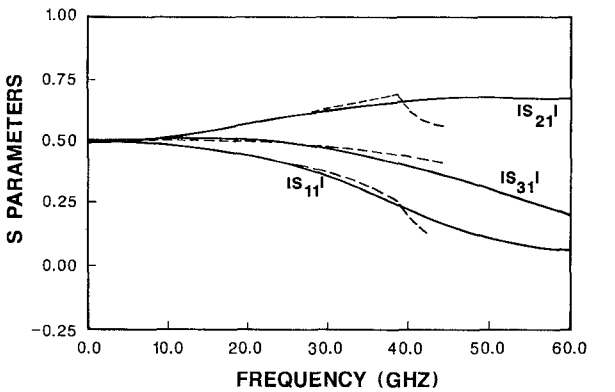

Fig. 14. Frequency-dependent S parameters of the microstrip cross-junction. Solid: time-domain result, dash: Mehran, $\epsilon_r = 9.7$, $h = 0.635$ mm, $W_1 = W_2 = 0.56$ mm [14].

The normalized frequency range used here corresponds to the frequencies from zero to 100 GHz for the structure concerned. The dc result of the time-domain calculation is very close to the quasi-static result of [4], the low frequency part is close to the experimental result of Edward ($W/H = 0.9$) [21], and the shape of the curve is similar to that of James and Henderson [16], which has too low a dc value though. The peak in the curve which appeared near the cutoff frequency of the first TE-type higher order mode of the microstrip has been predicted in [3].

B. Microstrip Cross-Junctions and T Junctions

Using a computation mesh domain similar to that for the open end (this time with $N_1 = 30$, $N_2 = 65$, $N_3 = 180$, and $\Delta h = H/8$), the symmetric microstrip cross-junctions and T junctions ($W_1 = W_2 = W = 0.6$ mm) under symmetric excitations are studied. Here the side boundary is given the same type of boundary treatment as for the end, since in this case sideways flow becomes another major direction of power flow.

Figs. 12 and 13 show the time-domain field distributions for the cross-junction and T junction. The Gaussian pulse which travels into the cross-junction is seen to split four ways after it hits the cross-junction. For the case of the T junction, a small amount of surface wave is observed to travel past the junction, as most of the energy is either reflected backward or transmitted sideways.

Figs. 14 and 15 plot the calculated S parameters for the cross- and T junctions (magnitudes only), together with the results of Mehran [14] as comparison. These results are calculated directly from the definition of each S parameter using the transformed time-domain fields in a way similar to the open-end case. The reference planes for the networks which represent the discontinuities are indicated in Fig. 1.

The independent S parameters for the cross-junction are S_{11}, S_{21}, and S_{31}. From Fig. 14, it is seen that these three S parameters all acquire the value 0.5 at dc and very low frequencies, indicating that the four branches of the cross-junction each get an equal 1/4 share of the total field energy; thus the U condition for the S matrix is well satisfied, and no (detectable) radiation occurs at those frequency ranges. The same is not true for higher frequency ranges.

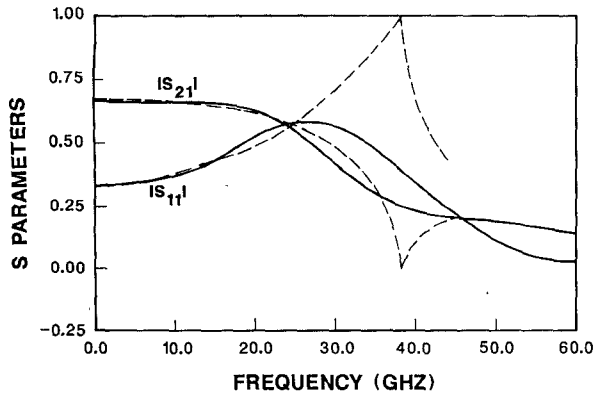

Fig. 15. Frequency-dependent S parameters of the microstrip T junction. Solid: time-domain result, dash: Mehran, $\epsilon_r = 9.7$, $h = 0.635$ mm, $W_1 = W_2 = 0.56$ mm [14].

The independent S parameters S_{11} and S_{21} for the T junction under symmetric excitation are plotted in Fig. 15. Again the U condition is checked to be satisfied in the very low frequency range.

From Figs. 14 and 15, it is seen that the time-domain results and the results of Mehran have very good agreement at dc and the lower frequency range. The discrepancies which occurred at very high frequencies are believed to be partly due to the fact that the waveguide model approach used in [14] is not able to take into account the radiation and surface wave generation effects which happened at higher frequency, and partly due to the fact that the time-domain results will not represent the exact dominant mode parameters after the inflection frequency, which is around 35 GHz for this configuration. The fact that the T junction results have earlier and larger discrepancy further confirmed this point, because here the surface wave becomes another reason for the waveguide model to fail, adding to the radiation loss.

C. Microstrip Step-in-Width and Gaps

Figs. 16 and 17 show the calculated time-domain fields and S parameters for the microstrip step-in-width ($W_1/H = 1.0$, $W_2/W_1 = 2.0$) using a mesh with size similar to that of T and cross-junction calculations. The S parameters for the step-in-width are defined as

$$S_{11} = \frac{V_{1\text{ref}}(f)}{V_{1\text{inc}}(f)} \tag{22}$$

$$S_{21} = \frac{\dfrac{V_{2\text{trans}}(f)}{\sqrt{Z_{02}(f)}}}{\dfrac{V_{1\text{inc}}(f)}{\sqrt{Z_{01}(f)}}} \tag{23}$$

$$S_{22} = \frac{V_{2\text{ref}}(f)}{V_{2\text{inc}}(f)} \tag{24}$$

$$S_{12} = S_{21} \tag{25}$$

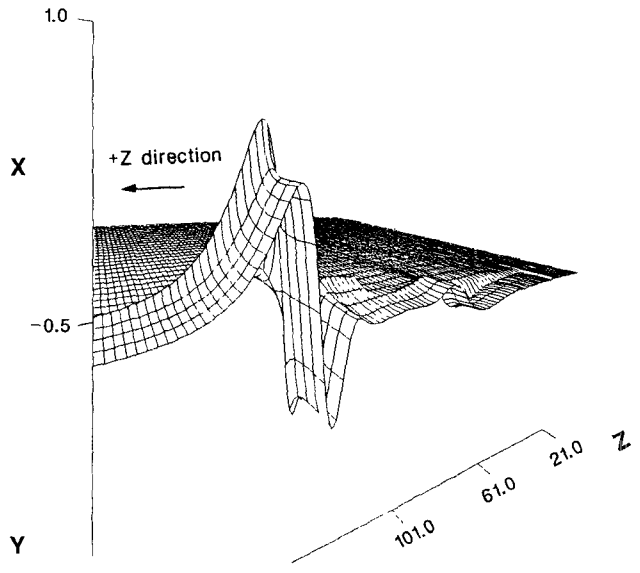

Fig. 16. Gaussian pulse propagation and reflection in the microstrip step-in-width structure: E_x component just underneath the strip.

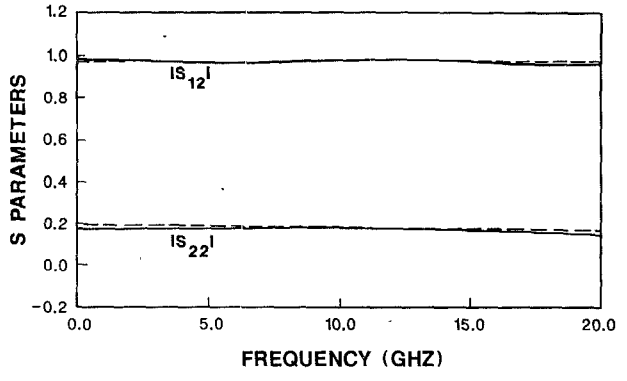

(a)

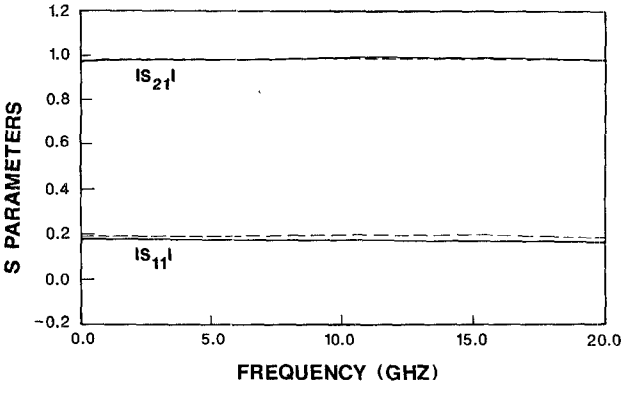

(b)

Fig. 17. Frequency-dependent S parameters of the microstrip step-in-width. Solid: time-domain result, dash: Koster and Jansen, $\epsilon_r = 10$ [33].

where $Z_{01}(f)$ and $Z_{02}(f)$ are the characteristic impedances of the microstrip lines connected to port 1 and 2 of the step, respectively, and are calculated in the same way as shown in [26].

The calculated frequency dependence of the S parameters of the step-in-width is quite flat over a large frequency

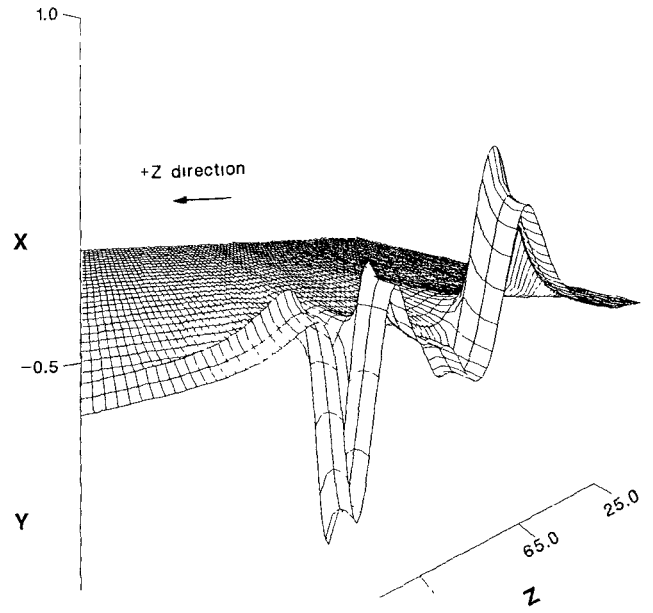

Fig. 18. Gaussian pulse propagation and reflection in the microstrip gap: E_x component just underneath the strip.

range. It is in good agreement with the result of Koster and Jansen [33].

Figs. 18 and 19 are the calculated time-domain fields and S parameters for the microstrip gap discontinuity ($S/H = 0.5$). The dc block characteristics of the gap are exhibited in the S parameter results.

IV. Conclusion

It has been shown that the time-domain finite difference approach is capable of calculating the dispersion characteristics of the microstrip discontinuities over a large frequency range. It is a very general method and can find wide applications in modeling various microwave components. Further investigations on different computer-memory-saving schemes will make this method more suitable for CAD purposes.

Appendix

To calculate the E_y and E_z components on the dielectric–air interface, we start with the Maxwell equation

$$\frac{\partial \vec{E}}{\partial t} = \frac{1}{\epsilon_i} \nabla \times \vec{H} \tag{A1}$$

where $i = 1, 2$ denotes the dielectric constant in the substrate and the air region, respectively. Taking the calculation of E_y as an example, we have, from (A1),

$$\frac{\partial E_y}{\partial t} = \frac{1}{\epsilon_i}\left(\frac{\partial H_x}{\partial z} - \frac{\partial H_z}{\partial x}\right). \tag{A2}$$

Since E_y, H_x and $\partial H_x/\partial z$ are continuous across the interface, it is very obvious that $\partial H_z/\partial x$ is discontinuous across the boundary; i.e., we can get from (A2)

$$\frac{1}{\epsilon_2}\left(\frac{\partial H_z}{\partial x}\right)_2 - \frac{1}{\epsilon_1}\left(\frac{\partial H_z}{\partial x}\right)_1 = \left(\frac{1}{\epsilon_2} - \frac{1}{\epsilon_1}\right)\frac{\partial H_x}{\partial z} \neq 0. \tag{A3}$$

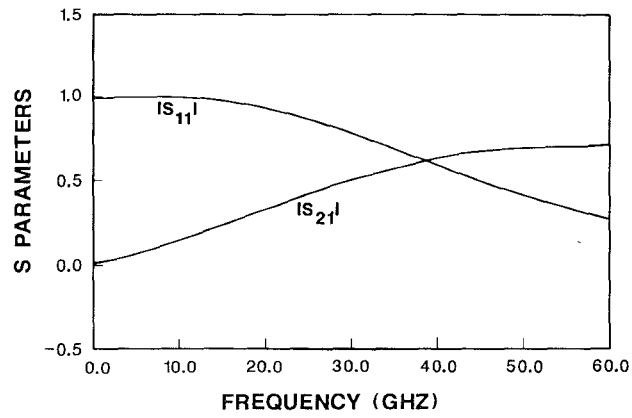

Fig. 19. Frequency-dependent S parameters of the microstrip gap.

Therefore on each side of the interface and at positions very close to the boundary, we can write

$$\epsilon_1 \frac{\partial E_y}{\partial t} = \frac{\partial H_x}{\partial z} - \left(\frac{\partial H_z}{\partial x}\right)_1$$
$$\epsilon_2 \frac{\partial E_y}{\partial t} = \frac{\partial H_x}{\partial z} - \left(\frac{\partial H_z}{\partial x}\right)_2. \tag{A4}$$

Approximate $(\partial H_z/\partial_x)_1$ and $(\partial H_z/\partial_x)_2$ by

$$\left(\frac{\partial H_z}{\partial x}\right)_1 \approx \frac{H_z(m) - H_z(m-1/2)}{\frac{\Delta x}{2}}$$
$$\left(\frac{\partial H_z}{\partial x}\right)_2 \approx \frac{H_z(m+1/2) - H_z(m)}{\frac{\Delta x}{2}} \tag{A5}$$

where m is assumed to be the position of the interface, and $m+1/2$ and $m-1/2$ denote the positions a half step above and below the interface, respectively.

Substituting (A5) into (A4), we get

$$H_z(m) \approx \frac{\epsilon_1}{\epsilon_1+\epsilon_2} H_z(m+1/2) + \frac{\epsilon_2}{\epsilon_1+\epsilon_2} H_z(m-1/2) + \frac{\epsilon_2-\epsilon_1}{\epsilon_1+\epsilon_2}\frac{\partial H_x}{\partial z}\Delta x/2. \tag{A6}$$

Substituting the $H_z(m)$ value of (A6) back into (A5), substituting the resulting (A5) into the two expressions in (A4), and adding the two together, we get

$$\frac{\epsilon_1+\epsilon_2}{2}\cdot\frac{\partial E_y}{\partial t} = \frac{\partial H_x}{\partial z} - \frac{H_z(m+1/2) - H_z(m-1/2)}{\Delta x} = \frac{\partial H_x}{\partial z} - \frac{\Delta H_z}{\Delta x}. \tag{A7}$$

Similarly, we get

$$\frac{\epsilon_1+\epsilon_2}{2}\cdot\frac{\partial E_z}{\partial t} = \frac{\Delta H_y}{\Delta x} - \frac{\partial H_x}{\partial y}. \tag{A8}$$

Thus we can further discretize (A7) and (A8) to calculate the tangential $\vec{E}$ components on the dielectric–air interface.

It is straightforward to show that this boundary approximation is of first order in space and second order in time.

REFERENCES

[1] J. J. Campbell, "Application of the solutions of certain boundary value problems to the symmetrical four-port junction and specially truncated bends in parallel-plate waveguides and balanced strip-transmission lines," *IEEE Trans. Microwave Theory Tech.*, vol. MTT-16, pp. 165–176, Mar. 1968.

[2] L. S. Napoli and J. J. Hughes, Foreshortening of microstrip open circuits on alumina substrate," *IEEE Trans. Microwave Theory Tech.*, vol. MTT-19, pp. 559–561, June 1971.

[3] D. S. James and S. H. Tse, "Microstrip end effects," *Electron. Lett.*, vol. 8, pp. 46–47, Jan. 27, 1972.

[4] P. Silvester and P. Benedek, "Equivalent capacitances of microstrip open circuits," *IEEE Trans. Microwave Theory Tech.*, vol. MTT-20, pp. 511–516, Aug. 1972.

[5] T. Itoh, R. Mittra, and R. D. Ward, "A method for computing edge capacitance of finite and semi-infinite microstrip lines," *IEEE Trans. Microwave Theory Tech.*, pp. 847–849, Dec. 1972.

[6] C. Gupta and A. Gopinath, "Equivalent circuit capacitance of microstrip step change in width," *IEEE Trans. Microwave Theory Tech.*, vol. MTT-25, pp. 819–822, Oct. 1977.

[7] A. A. F. Thomson and A. A. Gopinath, "Calculation of microstrip discontinuity inductances," *IEEE Trans. Microwave Theory Tech.*, vol. MTT-23, pp. 648–655, Aug. 1975.

[8] P. Stouten, "Equivalent capacitances of T junctions," *Electron. Lett.*, vol. 9, pp. 552–553, Nov. 1973.

[9] I. Wolff, A. G. Kompa, and R. Mehran, "Calculation method for microstrip discontinuities and T-junctions," *Electron. Lett.*, vol. 8, pp. 177, Apr. 1972.

[10] P. Silvester and P. Benedek, "Microstrip discontinuity capacitances for right-angle bends, T junctions, and crossings," *IEEE Trans. Microwave Theory Tech.*, vol. MTT-21, pp. 341–346, May 1973.

[11] M. Maeda, "An analysis of gap in microstrip transmission lines," *IEEE Trans. Microwave Theory Tech.*, vol. MTT-20, pp. 390–396, June 1972.

[12] A. Farrar and A. T. Adams, "Matrix method for microstrip three-dimensional problems," *IEEE Trans. Microwave Theory Tech.*, vol. MTT-20, pp. 497–504, Aug. 1972.

[13] G. Kompa and R. Mehran, "Planar waveguide model for calculating microstrip components," *Electron. Lett.*, vol. 11, pp. 459–460, Dept. 1975.

[14] R. Mehran, "The frequency-dependent scattering matrix of microstrip right-angle bends, T-junctions and crossings," *Arch. Elek. Übertragung.*, vol. 29, pp. 454–460, Nov. 1975.

[15] W. Menzel and I. Wolff, "A method for calculating the frequency dependent properties of microstrip discontinuities," *IEEE Trans. Microwave Theory Tech.*, vol. MTT-25, pp. 107–112, Feb. 1977.

[16] J. R. James and A. Henderson, "High-frequency behavior of microstrip open-circuit terminations," *IEE J. Microwave Opt. Acoust.*, vol. 3, pp. 205–211, Sept. 1979.

[17] R. H. Jansen, "The spectral-domain approach for microwave integrated circuits," *IEEE Trans. Microwave Theory Tech.*, vol. MTT-33, pp. 1043–1056, Oct. 1985.

[18] R. H. Jansen, "Hybrid mode analysis of end effects of planar microwave and millimeterwave transmission lines," *Proc. Inst. Elec. Eng.*, vol. 128, pt. H, no. 2, pp. 77–86, Apr. 1981.

[19] J. S. Hornsby, "Full-wave analysis of microstrip resonator and open-circuit end effect," *Proc. Inst. Elec. Eng.*, vol. 129, pt. H, no. 6, pp. 338–341, Dec. 1982.

[20] R. W. Jackson and D. M. Pozar, "Full-wave analysis of microstrip open-end and gap discontinuities," *IEEE Trans. Microwave Theory Tech.*, vol. MTT-33, pp. 1036–1042, Oct. 1985.

[21] P. B. Katehi and N. G. Alexopoulos, "Frequency-dependent characteristics of microstrip discontinuities in millimeter-wave integrated circuit," *IEEE Trans. Microwave Theory Tech.*, vol. MTT-33, pp. 1029–1035, Oct. 1985.

[22] K. S. Yee, "Numerical solution of initial boundary value problems involving Maxwell's equations in isotropic media," *IEEE Trans. Antennas Propagat.*, vol. AP-14, pp. 302–307, May 1966.

[23] A. Taflove and M. E. Brodwin, "Numerical solution of steady-state electromagnetic scattering problems using the time-dependent Maxwell's equations," *IEEE Trans. Microwave Theory Tech.*, vol. MTT-23, pp. 623–630, 1975.

[24] S. Koike, N. Yoshida, and I. Fukai, "Transient analysis of microstrip gap in three-dimensional space," *IEEE Trans. Microwave Theory Tech.*, vol. MTT-33, pp. 726–730, Aug. 1985.

[25] S. Koike, N. Yoshida, and I. Fukai, "Transient analysis of coupling between crossing lines in three-dimensional space," *IEEE Trans. Microwave Theory Tech.*, vol. MTT-35, pp. 67–71, Jan. 1987.

[26] X. Zhang, J. Fang, K. K. Mei, and Y. Liu, "Calculation of the dispersive characteristics of microstrips by the time-domain finite difference method," *IEEE Trans. Microwave Theory Tech.*, vol. MTT-36, pp. 263–267, Feb. 1988.

[27] L. Lapidus and G. H. Pinder, *Numerical Solution of Partial Differential Equations in Science and Engineering.* New York: Wiley, 1982.

[28] J. Fang, X. Zhang, K. K. Mei, and Y. Liu, "Time domain computation and numerical dispersion," presented at XXIInd General Assembly of the International Union of Radio Science, Tel Aviv, Israel, Aug. 24–Sept. 2, 1987.

[29] X. Zhang, "Time-domain finite difference calculation of the frequency-dependent characteristics of the microstrip discontinuities," master's report, Dept. EECS, University of California, Berkeley, Dec. 1987.

[30] K. K. Mei and J. Fang, "A super-absorption boundary algorithm for one dimensional wave equations," submitted to *J. Comput. Phys.*

[31] C. C. Lin, "Numerical modeling of two-dimensional time domain electromagnetic scattering by underground inhomogeneities," Ph.D dissertation, Dept. EECS, University of California, Berkeley, 1985.

[32] K. C. Gupta, R. Garg, and I. J. Bahl, *Microstrip Lines and Slotlines.* Dedham, MA: Artech House, 1979.

[33] N. H. L. Koster and R. H. Jansen, "The microstrip step discontinuity: A revised description," *IEEE Trans. Microwave Theory Tech.*, vol. MTT-34, pp. 213–223, Feb. 1986.

✠

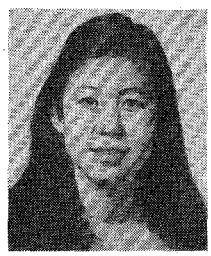

Xiaolei Zhang was born in Beijing, People's Republic of China, on April 1, 1963. She received the B.S. degree in electrical engineering in 1985 from Tsinghua University, Beijing, and the M.S. degree in electrical engineering from the University of California at Berkeley in December 1987.

She is now studying for the Ph.D. degree in the Department of Electrical Engineering and Computer Sciences at Berkeley. Her current research interests are in computer-aided passive microwave component modeling and numerical methods for solving electromagnetic problems.

✠

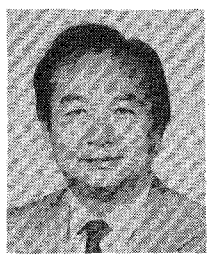

Kenneth K. Mei (S'61–M'63–SM'76–F'79) received the B.S.E.E., M.S., and Ph.D. degrees in electrical engineering from the University of Wisconsin, Madison, in 1959, 1960, and 1962, respectively.

He became a member of the faculty of the Department of Electrical Engineering and Computer Sciences of the University of California at Berkely in 1962. He is now a Professor there. His main areas of interest are antennas, scattering, and numerical methods in solving electromagnetic problems.

Dr. Mei received the best paper award and honorable mention of the best paper award in 1967 and 1975, respectively, from the IEEE Antennas and Propagation Society. He is a member of URSI/USNC. He served as a member of Adcom of the IEEE Antennas and Propagation Society and as an Associate Editor of its TRANSACTIONS.